Materials Research. 2024; 27:e20230442
DOI: https://doi.org/10.1590/1980-5373-MR-2023-0442

Microstructural Analysis of Partially Diluted Zones in Dissimilar Cladding: EBSD Insights on AWS E 309L Alloy via MIG Process in Single- and Double-Layer Depositions on ASTM A36 Steel

William Constantino da Silva[a]*, Rubens Maribondo do Nascimento[a], Nicolau Apoena Castro[b], Celina Leal Mendes Silva[c]

[a]*Universidade Federal do Rio Grande do Norte, Programa de Pós-Graduação em Ciência e Engenharia de Materiais, Natal, RN, Brasil.*
[b]*Universidade Federal do Rio Grande do Norte, Programa de Pós-Graduação em Engenharia Mecânica, Natal, RN, Brasil.*
[c]*Universidade da Amazônia, Departamento de Engenharia Mecânica, Belém, PA, Brasil.*

Received: October 08, 2023; Revised: February 09, 2024; Accepted: February 21, 2024

The surge in deep and ultra-deep water oil exploration in Brazil, particularly in the pre-salt layer, necessitates the advancement of materials and engineering components to meet sectoral challenges. To enhance the longevity and corrosion resistance of pipelines and structures, welded cladding of stainless alloys onto structural steels has been deployed. However, dissimilar welding often leads to the formation of Partially Diluted Zones (PDZ), marked by discontinuous, high-hardness regions at the interface. This study employs Electron Microscopy via Backscattered Electron Diffraction (EBSD) to characterize these zones, addressing limitations in conventional metallographic techniques. By cladding ASTM A36 steel test plates with AWS E 309L (309L stainless steel) through automated MIG welding, metallurgical-mechanical properties were assessed using Field Emission Scanning Electron Microscopy (FEG-SEM), EBSD, SEM-EDS, and Vickers Microhardness. The Heat-Affected Zone (HAZ) displayed low hardness, while the PDZ exhibited varied morphologies with significant concentrations of iron, chromium, and nickel, accompanied by elevated microhardness and a characteristic martensitic microstructure. In comparison between single and double-layer depositions, the latter substantially reduced hardness in the PDZ and HAZ. This study provides critical insights into the microstructural attributes of welded cladding, offering valuable guidance for optimizing materials in deepwater applications.

Keywords: *309L Stainless Steel, Dissimilar Welding, PDZ, EBSD.*

1. Introduction

The demand for oil and its derivatives, coupled with the need for greater productivity, has driven the oil and gas sector to explore deep waters along the Brazilian coast. This exploration has become a significant engineering challenge due to factors such as the pre-salt layer's geographic and geological characteristics, including distance from the coastline, water depth, and well drilling[1]. To withstand the corrosive nature of this environment, it is necessary to use materials with excellent corrosion resistance properties, such as low-carbon stainless steel alloys. However, these materials can be costly, leading to the use of cladding techniques to coat structural steels with austenitic stainless alloys like the 309L series stainless steel[2].

Cladding welding, using the AWS E 309L alloy, aims to optimize the cost-effectiveness of manufacturing components for specific applications that require resistance to the corrosive environment. This process involves the deposition of one or more layers of a corrosion-resistant alloy onto the surface of the structural steel component or equipment[3]. However, cladding dissimilar materials presents complex challenges compared to joining similar metals, including controlling dilution and the formation of metastable micro-constituents[4].

In the context of stainless-steel cladding deposited on structural steels, extensive investigations have been conducted. Karimi et al.[5] delved into fusion zone (FZ) structure and the mechanical properties of welded claddings involving 2205 stainless steel and A516 carbon steel. The study unveiled a FZ microstructure characterized by a distribution of ferrite-austenite originating from the duplex stainless steel, influenced by varying cooling and heating cycles.

Sun et al.[6] identified mechanical incompatibilities at the cladding interface of stainless steel-carbon steel composite plates, specifically between ferrite and martensite. This incompatibility resulted in stress concentration and the development of interface cracks. In a separate study, Zhang et al.[7] reported a parabolic trend in the growth behavior of the intermetallic compound layer between decarburized carbon steel and carburized stainless steel. Yu et al.[8] addressed the enhancement of shear strength in the interface of stainless steel-carbon steel composite plates through the development of a rolling process.

*e-mail: williamcs09@gmail.com

Thus, the interfacial region between the filler metal (cladding) and the base metal (substrate) is of great interest in dissimilar welding due to significant microstructural and mechanical changes along the fusion line of welded components. These changes are influenced by factors such as thermal input, compositional gradients, and the formation of critical high hardness regions, which can lead to detachment problems, loss of toughness, and corrosion phenomena[4,9]. The solidification process results in the formation of type II contours and Partially Diluted Zones (PDZ) due to the partial mixture between the filler metal and the base metal with different chemical compositions[10,11].

Regarding the morphologies of PDZs, such as beaches, swirls, and islands, these originate due to the convective movement of the liquid fusion pool in contact with the portion of the substrate melted by the welding energy, followed by partial solidification. However, it is important to note that this process does not occur continuously and linearly along the bonding zone, exhibiting preferential regions for the formation of these macrosegregations. Specifically, in the central portion of the weld bead, the presence of beach-type PDZs is predominantly observed. This phenomenon results from a stagnant melted layer of the substrate that did not mix with the filler metal during the welding process. On the other hand, morphologies such as "swirls" and "islands" are primarily found in the vicinity of the interpass regions of the beads composing the coating[12,13].

These PDZs morphologies may appear at the interface of a coated component. However, it is widely acknowledged that the predominant section of the interface between the austenitic filler metal and ferritic base metal does not exhibit the development of Partially Diluted Zones. The interface is distinctly defined, devoid of any signs of martensitic microstructure formation or localized hardness increase. Consequently, PDZs are identified as hard, small, and discontinuous regions[14].

Research conducted by Omar[15] regarding the impact of welding parameters on the formation of PDZs in dissimilar coatings yielded notable insights:

- All welding parameters possess the capability to either amplify or diminish the extent of the formed hard zones. Variations in preheating temperature and base metal thickness directly impact the hardness values manifested in the cladding interface.
- Dissimilar welds involving base metals with thicknesses below 4.8 mm exhibited the minimal occurrence of formed hard zones in comparison to dissimilar welds in thicker base metals, employing the same welding parameters.
- Omar suggests the existence of an optimal cooling rate for his experiment. Once exceeded (through an increase in preheating/interpass temperature or an increase in welding energy), this will result in an increased formation of hard zones due to the precipitation of intermetallic phases. Similarly, an increase in the cooling rate beyond the specified range will promote an increase in the formation of hard zones due to the formation of a martensitic structure.

While low-carbon stainless alloys are commonly used in cladding structural carbon steels for their corrosion resistance, further investigation into the formation and influence of ZPD is necessary to address the metallurgical challenges in the oil and gas industry[16]. This study aims to enhance the understanding of the metallurgical phenomenon of PDZs formed during cladding welding of dissimilar metals. Microanalysis techniques such as energy dispersive X-ray spectroscopy (EDS), backscattered electron diffraction (EBSD), and Vickers microhardness will be employed for phase identification and microstructural-mechanical characterization of these components. Through these techniques, a detailed observation of the microstructure in dissimilar claddings can be achieved.

2. Experimental Procedure

The base metal used as substrate was ASTM A36 steel in the form of plates with dimensions: 3/8" x 5" x 8" (Inch). The wire-electrode AWS E 309L alloy (309L stainless steel) with ø 1.2 mm was used as filler metal (cladding), protected by pure argon (commercial grade).

The cladding welding parameters are presented in Table 1.

The welding deposition was carried out using the conventional MIG process with a constant voltage mode and linear passes. Monitoring of voltage, current, and welding feed speed was facilitated by a multiprocess electronic welding power source connected to a data acquisition system. This allowed for the measurement of instantaneous energy as a response variable. The torch movement was automated using a displacement system.

Table 1. MIG cladding parameters.

WELDING PARAMETERS		
Voltage [V]		27
Stick Out [mm]		17
Welding Speed [mm/min]		300
Wire Feed Speed [m/min]		6
Heat Input [J/mm]		31.0
Interpass Temperature [°C]		< 100
Shielding Gas	Type	Argon
	Purity [%]	99.998
	Flow Rate [L/min]	15

The claddings, illustrated in schematic drawings (Figure 1a and 1b), were fabricated in both single-layer and double-layer configurations. In the single-layer cladding, welding beads were deposited side by side, while in the double-layer cladding, subsequent beads overlapped the previous ones. The interpass temperature was maintained below 100°C. This approach ensured a uniform distribution of the deposited metal, leading to improved metallurgical and mechanical properties of the cladding component. Careful selection of welding parameters was vital in ensuring the quality of the obtained cladding.

After the cladding deposition, cross sections of each test plate were prepared for microstructural analysis. The focus of the analysis was the interface between the cladding and the substrate, specifically the PDZ. The aim was to characterize the microstructure and chemical composition in this region to identify potentially detrimental areas to the mechanical properties and corrosion resistance of the cladding.

Vickers microhardness measurements were carried out according to ASTM E 384 standard[17]. The objective was to assess the mechanical behavior of different zones within the material and identify high hardness zones in the PDZs. Indentations were made along the cross section of the coated component, with regular spacing of 250 µm. The indentations covered the interface between the filler metal (FM) and the base metal (BM), entering the cladding (with 20 indentations). The same procedure was repeated on the BM (with 15 indentations), spanning the Heat-Affected Zone (HAZ), Coarse Grain Zone (CGZ), and Fine Grain Zone (FGZ). A load of 50 g was applied for 15 seconds during the indentation process.

3. Results and Discussion

This study focuses on the challenging interfacial region between the cladding and the low alloy steel in weld cladding components. The objective is to investigate the correlation between overlapping cladding layers and the metallurgical and mechanical properties of the welded component using a stainless alloy.

SEM-EDS analysis of the PDZ, base metal, and filler metal used in the single-layer 309L stainless steel cladding is presented in Figure 2. The image reveals the continuous formation of the PDZ, characterized by a "beach" morphology.

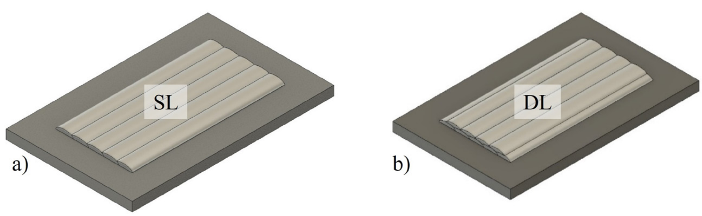

Figure 1. Schematic drawing of a single-layer (a) and double-layer cladding deposition (b).

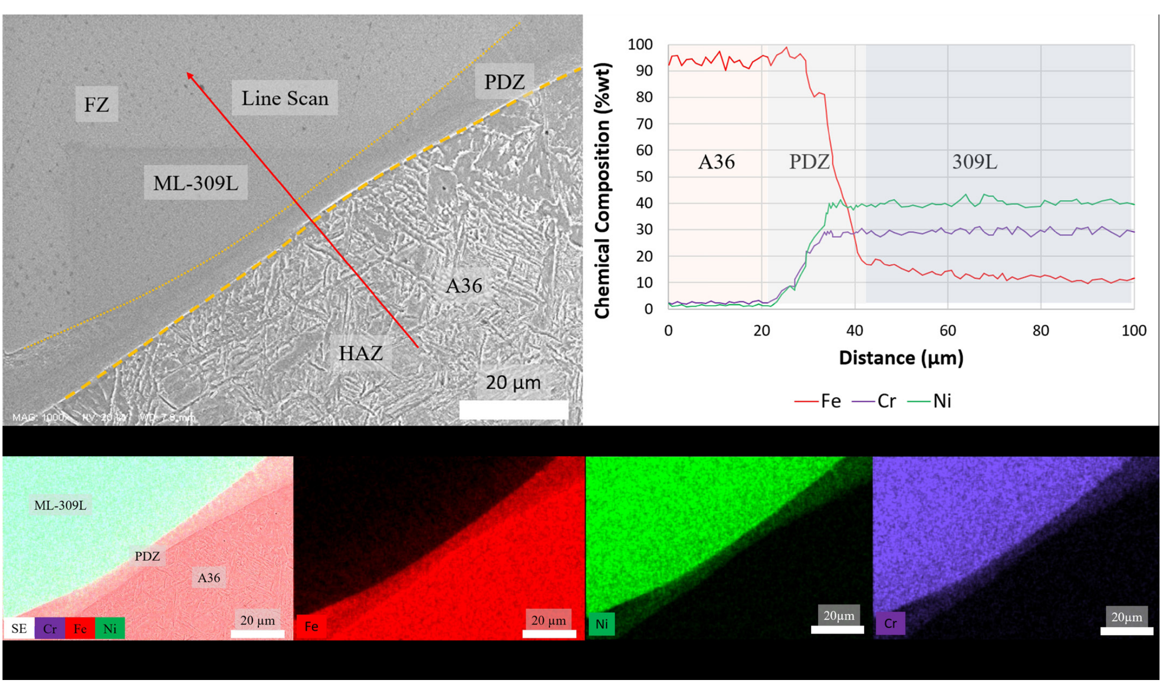

Figure 2. Line scan (a) compositional profile graph (b) area scan (c) of the chemical elements via EDS in single-layer dissimilar cladding with AWS E 309L alloy on ASTM A36 steel showing the transition region between the filler metal and the base metal. 1000x magnification.

This region separates the base metal (A36 steel) from the cladding (309L stainless steel), which underwent complete melting during the MIG welding process.

Figure 2a illustrates an electron microscopy image obtained during microanalysis using energy dispersive spectroscopy (EDS). Both line scan and mapping analysis were conducted to examine the distribution of chemical elements in the cladding interface. The image displays distinct regions, including the cladding, substrate, melting line, and a dotted line demarcating the Partially Diluted Zone. The red arrow indicates the line scan path during the analysis.

The PDZ, with an approximate thickness of 12 µm, spans the entire interface in the employed soldering condition (Figure 2b). EDS chemical mapping reveals a higher Fe content in the base metal (Figure 2c). The deposition of the liquid filler metal in contact with the base metal leads to dilution in the PDZ, resulting in a reduction of Fe content and the presence of Ni and Cr.

The microanalysis of chemical composition by line scan (Figure 2b) along a 100 µm analysis line demonstrates the formation of a PDZ with a thickness of approximately 10 to 15 µm. This region introduces alterations in the balance of chemical elements and the structure of the metals, facilitating the metallurgical bonding of the system. However, it is important to note that this region may contain metastable microconstituents and could be undesired in certain applications.

The mapping of chemical elements in an area by EDS can be observed in Figure 2c. The combined mapping of Fe, Cr and Ni elements is presented in the first analysis. In the other images, each microanalysis is observed with emphasis on each element individually. It is possible to notice a well-defined interface separating the cladding from the substrate. However, the Fe scan reveals that this element manages to diffuse beyond the PDZ and penetrate the filler metal, impoverishing the cladding alloy and making it more susceptible to corrosive phenomena.

In Figure 3, there is a graph and an image generated by SEM-EDS of the interface of the dual-layer deposited stainless steel 309L coating. It also depicts a PDZ with the morphology we refer to as “beach,” separating the base metal (A36 steel) from the molten filler material in the MIG welding deposition process.

Firstly, it is emphasized that the EDS analyses for all samples covering all test conditions were performed at similar locations — the central portion of the weld bead —to ensure a standardized evaluation condition, as the thickness of the ZPD varies along the fusion line.

In Figure 3, it can be observed that the ZPD is narrower and more discreet when compared to the ZPD formed with single-layer deposition. This reduction in ZPD may have been directly influenced by the welding energy imposed by the deposition of passes from the second layer, which promoted a rearrangement in the distribution of chemical elements in the interfacial region and the tempering of the microstructure in the HAZ on the substrate. Chemical mapping conducted by EDS highlighted that the base metal exhibits a higher iron content compared to the percentage presented by the filler metal. Nickel and chromium are well-defined in the coating material (Figure 3c). Taking into account the dilution of chemical elements in the ZPD due to the temperatures involved in the process and the compositional gradient, there is a percentage reduction in iron and the presence of nickel and chromium, indicating the dilution process of the base metal mixing with the filler metal.

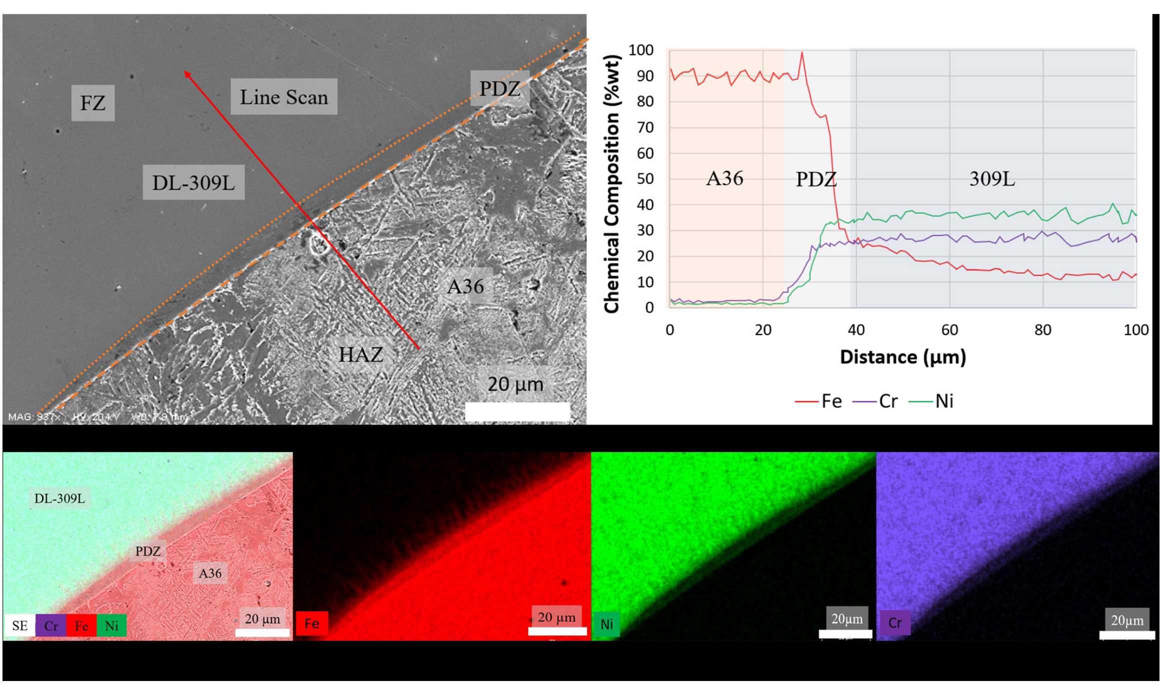

Figure 3. Line scan (a) compositional profile graph and (b) area scan (c) Chemical element mapping via EDS in double-layer dissimilar cladding with AWS E 309L alloy on ASTM A36 steel, illustrating the transition region between the filler metal and the base metal. Magnification: 1000x.

Regarding the microstructure of the HAZ, it appears in the form of acicular grains. The composition analysis via Line Scan (Figure 3a) over 100 µm also highlights the formation of the ZPD, as a region with a thickness between 8 to 10 µm, quantitatively presenting the gradient of chemical elements at the interface of the coated component.

The analysis of the grain microstructure was performed using the Electron Backscattered Diffraction (EBSD) technique in a Field Emission Scanning Electron Microscope (FEG-SEM). This technique was especially useful for the case in question, as it enabled mapping the crystallographic orientation and microstructure of the grains without the need to use metallographic reagents, which is important due to the high corrosion resistance of the alloy used as filler metal in the dissimilar claddings.

Therefore, the EBSD technique is able to provide distribution maps of crystallographic orientations from which it is possible to observe the existence of several planes with different orientations and with BCC and FCC crystalline structures[18].

The micrograph illustrated in Figure 3 was obtained by EBSD and shows the mapping of crystalline phases at the interface of the cladding component (Figure 4a) and the inverse pole figure (IPF) map (Figure 4b).

Figure 4a shows diffraction patterns obtained by measuring backscattered electrons from the sample surface, allowing for the determination of the crystalline structures of individual grains. The blue region represents the FCC structure of the 309L stainless steel alloy cladding layer, while the red region corresponds to the BCC ferritic structure of the A36 steel substrate.

The image reveals the formation of a "beach" type PDZ along the interface between the base metal (BM) and the filler metal (FM) from the steel substrate. Additionally, it is evident that a portion of the substrate (red region) is fully diffused into the cladding, creating a PDZ morphology referred to as an "island." The PDZ possesses the same crystalline structure as the base metal, and the EDS results indicate the presence of dilution gradients in this zone.

Based on these observations, it is assumed that the diffusion of chemical elements primarily affects the chemical composition and subsequent hardenability of these regions, without significantly altering the ferritic matrix structure of the steel.

From the IPF map (Figure 4b) obtained through EBSD at 500x magnification, it was observed that the base metal experienced significant local dilution with the filler metal, leading to the formation of a substantial PDZ in the analyzed region. Figure 3 clearly depicts the development of a "Beach" type PDZ, which extends continuously along the Bonding Zone (BZ) and exhibits a refined microstructure characteristic of martensitic structures (M).

The presence of martensite microstructure is also evident in the PDZ regions of the "Island" type, located within the molten mass of the filler metal. These regions contribute to the increased susceptibility of the cladding component to cracking and detachment due to their high hardness.

Additionally, acicular grains with bainite morphologies (B) can be observed in the Heat-Affected Zone (HAZ). These morphologies result from the welding energy generated by the electric welding arc and the subsequent high-temperature melting of the filler metal, which promotes heat treatment within the substrate microstructure.

Figure 5 shows the Phase Map (a) and the IPF Map (b) generated by EBSD with 500x magnification of the cladding interface regarding the double layer deposition with the 309L alloy.

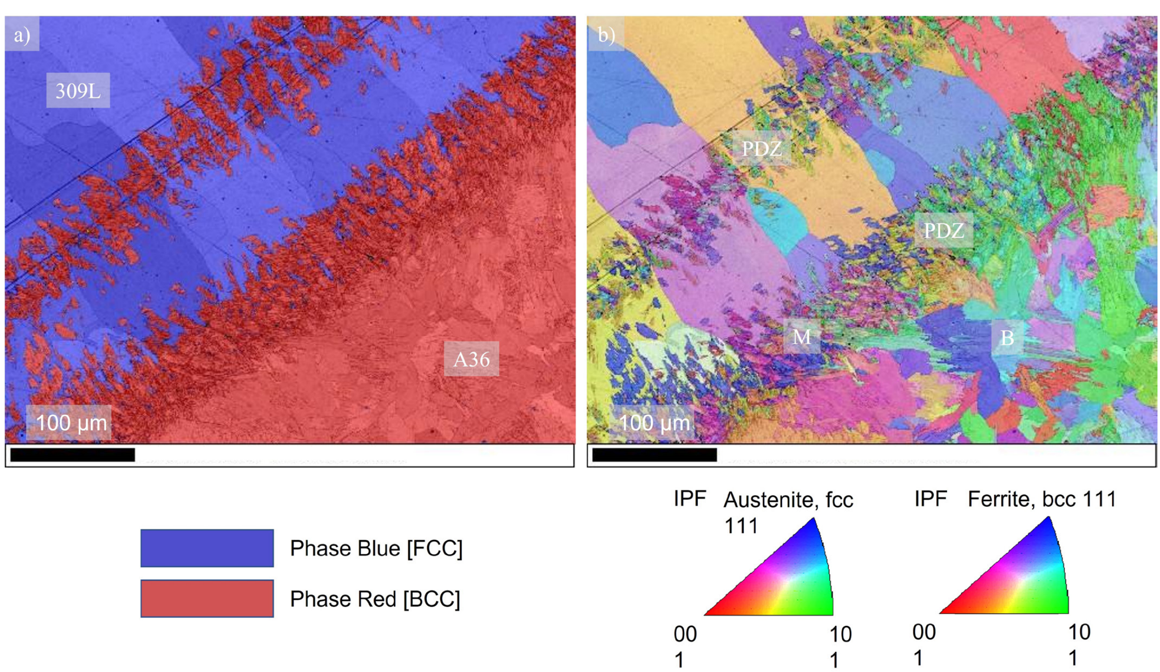

Figure 4. Phase Map (a) and IPF Map (b) via EBSD of the 309L stainless steel cladding deposited by the MIG process in a single layer on ASTM A36 steel. 500x magnification.

Analogously to that obtained in the single-layer deposition, the double-layer cladding was also characterized by the backscattered electron diffraction patterns of the different crystalline phases of the welded component. One can observe separation of the ferritic phases (BCC) in red from the substrate, from the austenitic phase (FCC) in blue from the stainless-steel cladding. A different PDZ morphology is observed in this micrograph than that presented in the single-layer deposition. In this case, the portion of the substrate entering the cladding and forming what is called a "swirl" is visualized, as well as small portions of the BM dispersed in the form of "islands" inside the austenitic filler metal mass.

The IPF map obtained through EBSD (Figure 5b) clearly shows the formation of a "Swirl" type PDZ that extends into the filler metal, exhibiting acicular grains within it. Adjacent to the PDZ, a highly refined martensitic microstructure is observed. The presence of martensite is also noted in the upper part of the PDZ. This indicates that the balance of chemical elements, with high iron content from the base metal and high alloy element content from the Cr-rich cladding, significantly increases the hardenability in these regions. The formation of metastable microconstituents, mainly martensite, is observed in these locations.

Furthermore, a transformation in the grains of the Heat-Affected Zone (HAZ) is observed. In the single-layer deposition, acicular ferrite and bainite were predominant, but in the current stage, the grains have transformed into equiaxed morphology, which is more thermodynamically stable. Although traces of bainite are still present, they are less significant.

The formation mechanism of the "Swirl" type PDZ (Figure 5) is influenced by the migration of a part of the substrate into the cladding, resulting in a region entirely surrounded by the filler metal. This PDZ exhibits two distinct microstructures: the central portion of the swirl displays the typical HAZ microstructure of the base metal, while the edges near the filler metal show a prevalence of martensite, primarily formed through dilution and cooling. The casing surrounding the swirl shows an increased planar growth region due to localized rapid cooling.

By analyzing the IPF images in Figures 4 and 5, the formation of beach, island, and swirl regions can be observed. The EBSD technique allows for the observation of a more refined microstructure in these highlighted regions, with the formation of acicular grains, which are typical of martensitic phases.

Comparing the IPF maps of the single-layer (Figure 4) and double-layer cladding (Figure 4), it can be seen that the single-layer cladding has a HAZ dominated by acicular grains, indicating significant hardness levels in these regions. On the other hand, the double-layer cladding displays a HAZ with the formation of equiaxed grains, resulting from the tempering effect induced by the thermal input from the second layer passes. This is beneficial for the performance of the weld cladding component in service. It is worth mentioning that the deposition of a second layer promotes refinement and tempering in the PDZ region of the first layer, as explained by Cozza[19] and Aguirre et al.[20]. The overlapping thermal cycles during the welding process lead to the formation of equiaxed grains instead of acicular grains in the preferred PDZ formation regions. As a result, the HAZ exhibits lower hardness and greater ductility.

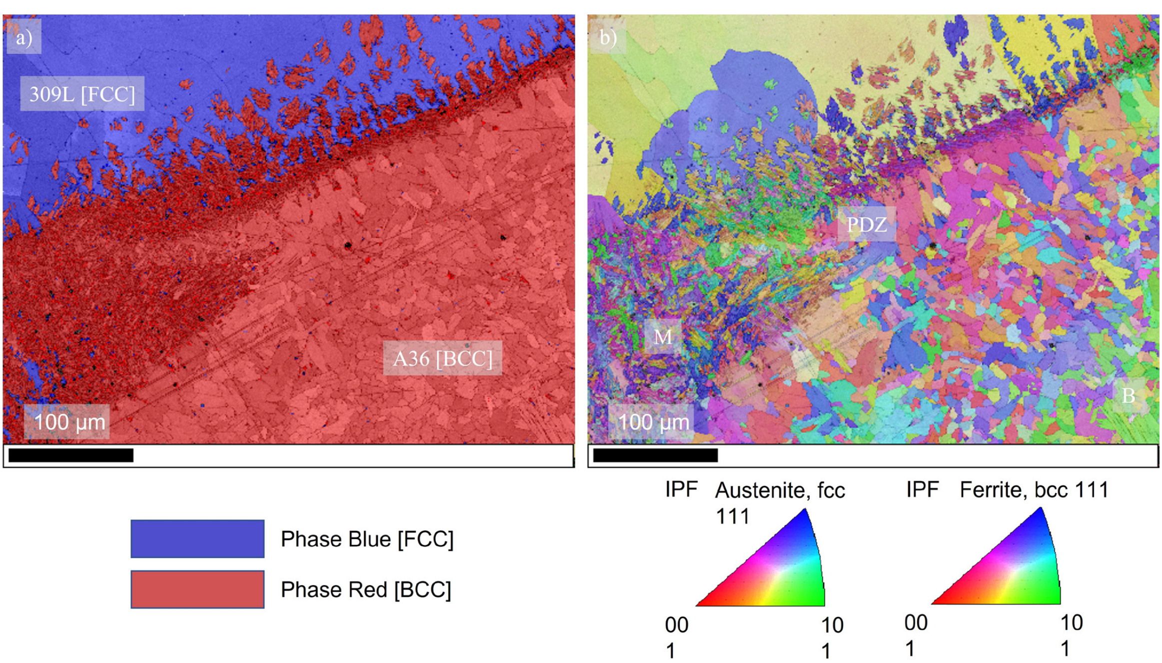

Figure 5. Phase Map (a) and IPF Map (b) via EBSD of the 309L stainless steel cladding deposited by the MIG process in a double layer on ASTM A36 steel. 500x magnification.

3.1. Microhardness profiles

In study weld cladding, the hardness of a cladding is the result of the chemical composition and the microstructure both impacted by the welding processes, as well as the welding energy imposed by the welding process, since the cladding and substrate are fused in the bonding zone (BZ) to promote their coalescence and an interaction between the materials. Thus, the microhardness profile is an important tool for characterizing weld cladding[21].

The microhardness profiles of the cross-section of single-layer (SL 309L) and double-layer (DL 309L) cladding samples were modeled in the present study. In analyzing the graph shown in Figure 6, an observable pattern for the two curves (SL 309L and DL 309L) is the significant increase in hardness levels in the region of the zero-millimeter distance, here representing the BZ between the cladding and the substrate, and therefore the PDZ of the cladding component.

According to studies presented by Kejelin[22], microhardness tests indicated the presence of PDZs with typically martensitic microstructures in the transition region between the cladding and the substrate; these are detrimental to the structural performance of the welded component. In turn, the main metallurgical problem found in welds of α-γ dissimilar metals is the formation of high hardness regions (which can exceed 400 HV) along the interface of the fusion line, which indicate the presence of martensite and therefore make the cladding component susceptible to failure in service. This is consistent with what was observed in the IPF maps images shown in Figures 4 and 5.

Cavalcante et al.[23] found similar microhardness results in α-γ dissimilar cladding using MAG welding. The authors reported the same tendency of this abrupt increase right after the zero line, jumping from values close to 220 HV in the cladding region, to values of approximately 330 HV in the regions close to the interface (BZ) of the substrate and the cladding.

Thus, it is possible to observe that there was a significant increase in the microhardness values for both curves in the interface region between the cladding and the substrate. This can be attributed to the formation of PDZ. According to Mota et al.[24], PDZs are macrosegregations inherent to the welding of dissimilar materials and are conducive to detachment of the cladding layer and to embrittlement due to the formation of carbides and martensitic structures.

There is proximity between the two curves in the cladding region to the left of 0 mm, from a maximum of approximately 240 HV in a double layer, to a minimum of approximately 205 HV (region with a drop in hardness of the cladding adjacent to the PDZ) in a single layer (SL 309L).

In comparing the two curves, it was possible to clearly identify a significant change in the pattern of the graphs, since a high hardness region was observed close to 360 HV (typical hardness of martensitic microstructures) in the PDZ of the single layer curve when compared with the double-layer deposition curve, which presented the lowest hardness peak in the PDZ region with about 310 HV.

In view of this, the influence of the double layer on the tendency to minimize the hardness levels in the BZ region and in the HAZ region of the base metal was observed. This may have occurred due to the heating provided by the thermal cycle of welding the upper layer, causing tempering of these high hardness regions to have occurred. This was reported by Oliveira and Miranda[25] in their study aiming to evaluate the effect of using the double layer technique when applied in welding ASTM A516 G70 structural steel.

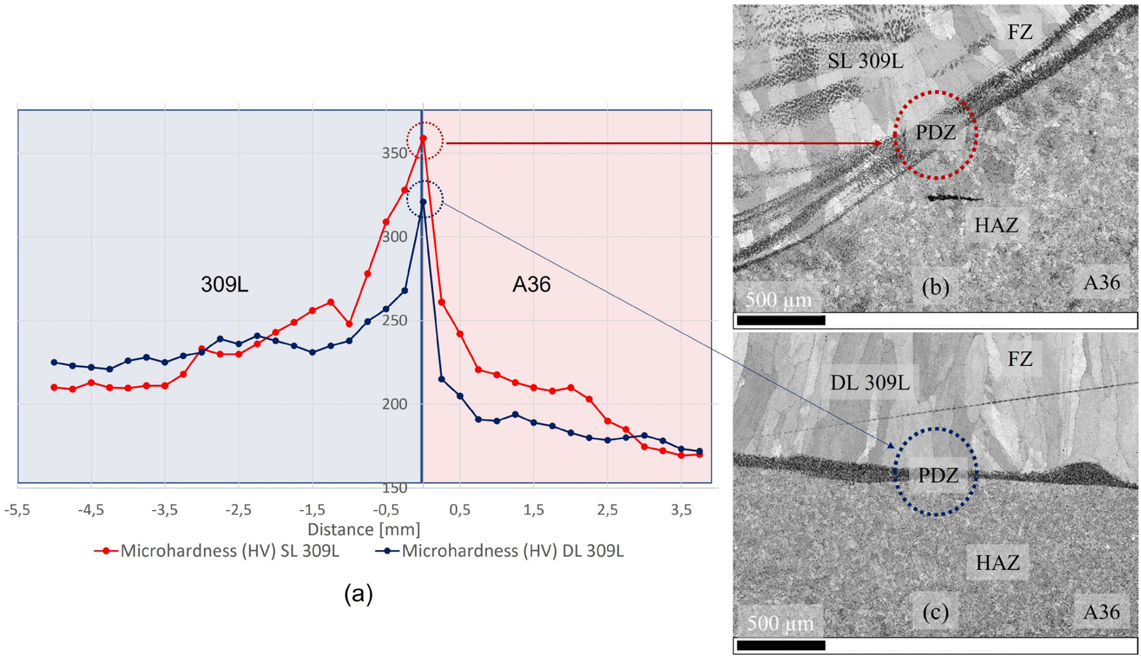

Figure 6. Comparative profile of Vickers microhardness (a) of cladding deposited by wire-electrode MIG welding from AWS E 309L alloy (309L stainless steel) on ASTM A 36 steel in single layer [SL] (b) and double layer [DL] (c).

The microstructural refinement obtained in the HAZ of the samples welded using the double layer technique was followed by microstructure tempering, which in turn suggests that this was obtained due to a greater number of passes performed in the technique. Although the steel is not the same as that used in the present work, it can be suggested that the same metallurgical phenomenon may have occurred in the test plates presented.

Microhardness values above 350 HV can be explained by the formation of PDZ. As reported by Sandes[26], PDZs are often associated with the formation of martensite, which originate during cooling in the welding process. In comparing the weld bead region of the samples, it is noted that the hardness values are in accordance with what is reported in the literature, which present an average of 220 HV and a maximum of 390 HV in the PDZ for austenitic alloys[27-29].

4. Conclusions

According to the results obtained, it is possible to conclude that:

- Considering the interfacial region between the filler metal (cladding) and the base metal (substrate) and based on the metallurgical characteristics presented, it was possible to observe that higher dilution levels directly contributed to forming Partially Diluted Zones (PDZ). These presents themselves in three distinct morphologies: beach, swirl and island.
- The formation of beach-type PDZs was more markedly observed in the single-layer coating, where the transition region of chemical elements in the fusion line between the filler metal and the base metal became apparent in mapping chemical elements via EDS.
- The morphology of swirls mainly occurred in the regions between the weld beads (interpass region) deposited in multipasses for formation the cladding. These morphologies occur due to the convection phenomena of the molten mass in the molten pool as a result of the partial detachment of the molten and unmixed substrate and its consequent migration into the cladding interior, followed by rapid solidification of this metal portion due to its higher melting temperature compared to the filler metal.
- It was also possible to observe along the fusion line that the swirl-type PDZs occurred in a punctual manner and in preferential regions (interpass regions), while the beach-type PDZs occurred continuously in the central region of the weld bead as a strip of structural/mechanical discontinuity along the fusion line; and that due to the high hardness, these can contribute to detaching of the cladding layer because of the tendency to nucleation and crack propagation.
- A significant influence was observed between the formation/microhardness of the PDZs as a function of the double layer technique. Thus, the PDZs in the cladding where single layer deposition was used were thicker and had higher hardness levels.
- Regarding the HAZ, the double layer technique also contributed to improve the mechanical properties of these regions, because the presence of equiaxed grains in the substrate was observed when compared to the cladding deposited in a single layer, thereby favoring a reduction in hardness levels in these areas thermally affected by the welding thermal cycle.

5. Acknowledgements

The authors would like to thank the *Coordenação de Aperfeiçoamento de Pessoal de Nível Superior* (*CAPES*) for the financial support provided for developing this research work.

6. References

1. Petrobras [homepage on the Internet]. 2023 [cited 2023 Oct 8]. Available from: petrobras.com.br
2. Zhang Q, Tang R, Yin K, Luo X, Zhang L. Corrosion behavior of Hastelloy C-276 in supercritical water. Corros Sci. 2009;51(9):2092-7.
3. Rowe MD, Nelson TW, Lippold JC. Hydrogen induced cracking along the fusion boundary of dissimilar metal welds. Weld J. 1999;78(2):31-7.
4. Wang JF, Sun QJ, Wang H, Liu JP, Feng JC. Effect of location on microstructure and mechanical properties of additive layer manufactured Inconel 625 using gas tungsten arc welding. Mater Sci Eng A. 2016;676:395-405.
5. Karimi A, Karimipour A, Akbari M, Razzaghi MM, Ghahderijani MJ. Investigating the mechanical properties and fusion zone microstructure of dissimilar laser weld joint of duplex 2205 stainless steel and A516 carbon steel. Opt Laser Technol. 2023;158(Pt A):108875.
6. Sun JH, Liu XF, Yang YH, Wang WJ. Interfacial gradient M7C3 carbides precipitation behavior and strengthening mechanisms of stainless steel/carbon steel clad plates. J Mater Res Technol. 2022;21:3476-88.
7. Zhang QD, Yu MY, Zhang BY, Li H. Growth behavior of interface microstructure between stainless steel and carbon steel during bonding process. Mater Today Commun. 2022;33:104647.
8. Yu WD, Jing YA, He XZ, Yang YN, Zhang MF, Cheng S, et al. An innovative process of clad teeming and rolling for preparing stainless steel/carbon steel clad plate. J Manuf Process. 2022;84:1428-37.
9. Wang Z, Xu B, Ye C. Study of martensite structures at the weld interface and fracture toughness of dissimilar metal joints. Weld J. 1993;72(8):397-402.
10. AWS: American Welding Society. Welding handbook: materials and applications. 9th ed. Miami: AWS; 2011. 695 p. (vol. 4).
11. Nelson T, Lippold J, Mills M. Nature and Evolution of the fusion boundary in ferritic-austenitic dissimilar metal welds. Part 2: on-cooling transformations. Weld Res Suppl. 2000;79(10):267s-77s.
12. Kumar S, Kumar S, Pandey C, Goyal A. Effect of post-weld heat treatment and dissimilar filler metal composition on the microstructural developments, and mechanical properties of gas tungsten arc welded joint of P91 steel. Int J Press Vessels Piping. 2021;191:104373. http://dx.doi.org/10.1016/j.ijpvp.2021.104373.
13. Kou S. Welding metallurgy. New York: John Wiley & Sons; 2003.
14. Kejelin NZ. Influência dos parâmetros de soldagem na formação de zonas parcialmente diluídas em soldas de metais dissimilares [dissertation]. Florianópolis: Programa de Pós-graduação em Ciência e Engenharia de Materiais, Universidade Federal de Santa Catarina; 2006.
15. Omar AA. Effects of welding parameters on hard zone formation at dissimilar metal welds. Weld J. 1998;77:1-8.
16. Elias MS. Avaliação metalúrgica da soldagem de revestimento inox austenítico sobre aço SAE 4130 [dissertation]. Campos dos Goytacazes: Laboratório de Materiais Avançados, Centro de Ciência e Tecnologia, Universidade Estadual do Norte Fluminense Darcy Ribeiro; 2013.

17. ASTM: American Society for Testing and Materials. ASTM E384: standard test method for microindentation hardness of materials. West Conshohocken: ASTM International; 2022.
18. Alam MK, Mehdi M, Urbanic RJ, Edrisy A. Electron Backscatter Diffraction (EBSD) analysis of laser-cladded AISI 420 martensitic stainless steel. Mater Charact. 2020;161:110138.
19. Cozza LM. Estudo da técnica da dupla camada na soldagem do aço A131 grau AH36 [dissertation]. Rio Grande: Universidade Federal do Rio Grande; 2018.
20. Aguirre HVM, Teixeira FR, Mota CAM, Nascimento AS. Avaliação de soldas dissimilares com a técnica da dupla camada utilizando os arames-eletrodos AWS ER 316L e ER NiCrMo-3 sobre o aço ASTM A182 F22. Rev Matéria. 2021;26(3):e13000.
21. Blau PJ. Microindentation hardness testing. In: ASM International. Friction, lubrification, and wear technology. Materials Park: ASM International; 1992. p. 787-96. (ASM Handbook; 18).
22. Kejelin NZ. Soldagem de revestimento de aços comuns C-Mn com superliga a base de níquel Inconel 625 [thesis]. Florianópolis: Programa de Pós-graduação em Engenharia Mecânica, Universidade Federal de Santa Catarina; 2012.
23. Cavalcante NE, Andrade TC, Pinheiro PHM, De Miranda HC, Motta MF, Aguiar WM. Estudo de procedimentos de soldagem MIG/MAG para aplicação de revestimentos de liga de níquel Inconel 625 em aço estrutural ASTM A387 Gr.11. Soldag Insp. 2016;21(1):70-82.
24. Mota CAM, Nascimento AS, Garcia DN, Silva DAS, Teixeira FR, Ferraresi VA. Revestimento de níquel depositado pela soldagem MIG e MIG com arame frio. Soldag Insp. 2016;21(4):483-96.
25. Oliveira GLG, Miranda HC. Efeito da aplicação da técnica da dupla camada sobre a microestrutura, microdureza e tensões residuais do aço estrutural ASTM A516 G70. In: 65º Congresso Anual da ABM; 2010; São Paulo. Anais. São Paulo: ABM; 2010. p. 3191-202.
26. Sandes S. Efeito do procedimento de soldagem nas propriedades de revestimentos metálicos de liga 625 pelo processo eletroescória [dissertation]. Rio de Janeiro: CEFET/RJ; 2016.
27. Dupont JN, Lippold JC, Kiser SD. Welding metallurgy of nickel-base alloys. New York: John Wiley & Sons; 2009.
28. Pfingstag ME, Muller IL, Schaeffer L. Avaliação em relação à corrosão-fadiga de juntas soldadas da liga Inconel 625. Cienc Tecnol Mater. 2010;22(3-4):65-70.
29. Constantino WS. Avaliação microestrutural de Zonas Parcialmente Diluídas obtidas por soldagem dissimilar empregando os metais de adição Inox 309L e Inconel 625 [dissertation]. Natal: Programa de Pós-graduação em Ciência e Engenharia de Materiais, Universidade Federal do Rio Grande do Norte; 2018.